Int J CARS (2010) 5 (Suppl 1):S229–S234
DOI 10.1007/s11548-010-0462-3

Registration of Cone-Beam CT and 3dMD Maxillodental Data Over Time

N. Bolandzadeh Fasaie[1], P. Boulanger[1], C. Flores-Mir[2]
[1]University of Alberta, Computing Science, Edmonton, Canada
[2]University of Alberta, Dentistry-Pharmacy Center, Edmonton, Canada

Keywords Maxillofacial Imaging · CBCT · 3dMD

Purpose

Explore a methodology for tracking hard and soft tissue variations that occur during orthodontic (craniofacial) treatment. Registered images obtained from Cone-Beam Computed Tomography (CBCT) along with 3dMD photogrammetry sensors could used to show teeth, jaw, and skin displacements during the treatment period. This method can be deployed for maxillofacial surgical planning as well as clinical evaluation of orthodontic treatments.

Methods

Six consecutive patients with adequate records were chosen from an ongoing clinical trial. Some were just untreated controls. Ethical approval was granted by the University of Alberta HREB. Multimodal images of CBCT and Photogrammetry were acquired two times within an 8-12 month period.

Imaging Modalities

A NewTom QR-DVT9000 scanner (Cone Beam Computed/Volumetric Tomography - CBCT) was used for reconstruction of volumetric images of hard tissues. Using square 2-dimensional array of detectors, this scanner deploys cone shaped rather than fan shaped X-ray beams to provide volumetric data of craniofacial regions. This technology has shown high accuracy for craniofacial regions [1].

The second imaging technology (3dMD) enables capturing external skin surfaces non-invasively. This technology relies on a stereo photogrammetry technique. Once three pairs of photographs are taken by adequately positioned cameras, a correspondence algorithm is used for recovering the 3D model. This algorithm employs unique random light patterns projected to the surface, and accomplishes its goals by triangulating the geometry of the surface in 3D. The 3dMD software then maps color information captured from color cameras onto the model. The result is a highly precise 3D colored model of the patients' facial skin.

Registration of Multimodal Data Obtained from CBCT and 3dMD

In order to register CBCT with 3dMD data, it is necessary to have reference points that would not scatter by the radiation beam and are clearly identifiable through both CBCT and 3dMD images. Therefore six Titanium spheres (diameter 6.5mm) were located on a head-band on patient's forehead during the imaging.

Rapidform, a commercial polygon processing software, consists of many implemented image processing algorithms that allow registration and segmentation for both CBCT and 3dMD polygonal data. To be able to register images, we should register the target points first. Hence, artificial spheres are fitted on the existing ones, and the spheres' centers are estimated using Rapidform. Through finding a transformation matrix between the spheres' centers, 3D models are matched [2]. In order to get a more accurate result, Fine registration, an implementation of Iterative Closest Points (ICP) algorithm, is used. Figure 1A and B show Data#4 registration for T1 and T2 respectively.

Segmentation and Registration of Jaws

Since the lower jaw moves independently from the upper head, it might be worthwhile to segment, register and analyze it independently.

For initiating lower jaws' registration procedure identifying natural landmarks are necessary. Since the landmarks should ideally stay in the same position from T1 to T2, they should be selected from areas that don't undergo growth changes in one-year period. Therefore, as shown in Figure 1C, nerve passage foramina and the inner cortical surface were used [3]. Then Initial and Fine registration is done whose result for Data#4 is shown in Fig. 1D.

Registration of Multimodal Data through Time

Using target points for the registration of CT with 3dMD images is challenging since there is no guarantee to hold the target points exactly in the same place. Instead, natural features of skull are used in this process. First, they should be easily identifiable in both CBCT and 3dMD. Second, these features should not be a subset of a growing part. Proposed points are illustrated in Figure 1E. The Initial and Fine registration have been applied whose result for Data#4 is shown in Fig. 1F.

Results

The step-by-step procedure for registration of jaws over time is explained below:

1. Manually segment the lower jaw polygonal data from the skull in T1 and T2.
2. For each time, segment three natural landmarks illustrated in Figure 1C.
3. Group the segmented regions with the rest of jaw.
4. Apply Initial and Fine registration methods.

Reproducibility

Once the registration results were obtained, all the data went through the whole procedure three times. The reproducibility of our method was assessed under the hypothesis that some specific areas in the lower jaw should remain mostly unchanged during the treatment, while the rest may have changed by treatment or growth.

Moreover, a diagram of normalized deviation distribution between T1 and T2 jaws is shown in Fig. 2. This measurement proves the effectiveness of proposed registration procedure. The Gaussian distribution centered at zero shows a greater number of points on T1 having smaller distance with their corresponding points on T2. This diagram is obtained from all six data, and shows the similarity and consistency of our methodology's results.

Conclusion

This study showed a complete procedure for registration of 3dMD photogrammetric data with CBCT images through time. Use of target points and the process of registration are explained. The criteria for choosing relatively stable landmarks on the skull have been discussed, appropriate features were selected, and a methodology for registration through time for jaws and skull has been presented. Moreover, the

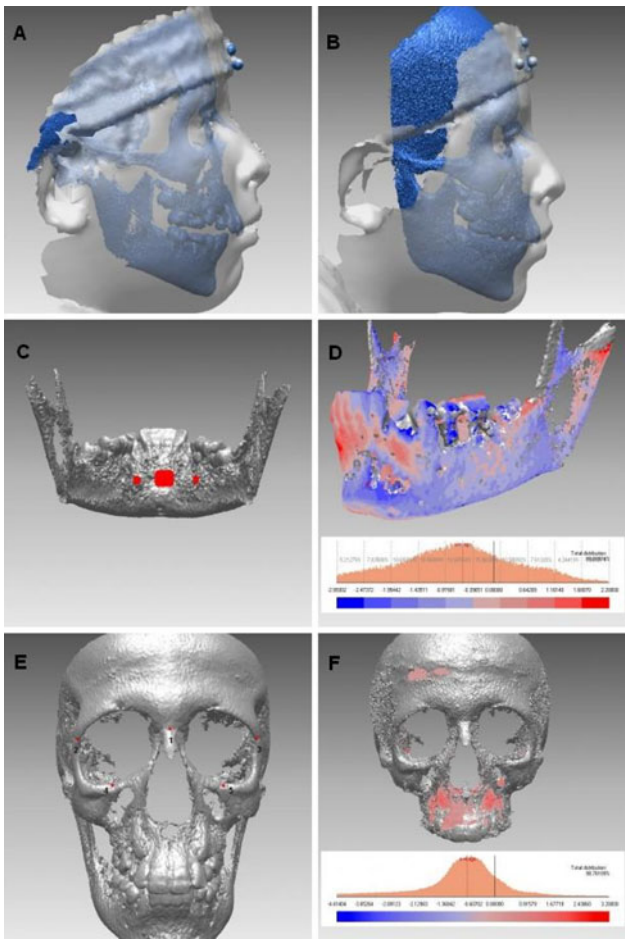

Fig. 1 A-B: Registration of CBCT and 3dMD at T1 and T2 respectively. C: Natural regions for jaw registration. D: Jaw registration of T1 and T2. E: Natural landmarks for registration of upper skull. F: Registered upper skulls of T1 and T2

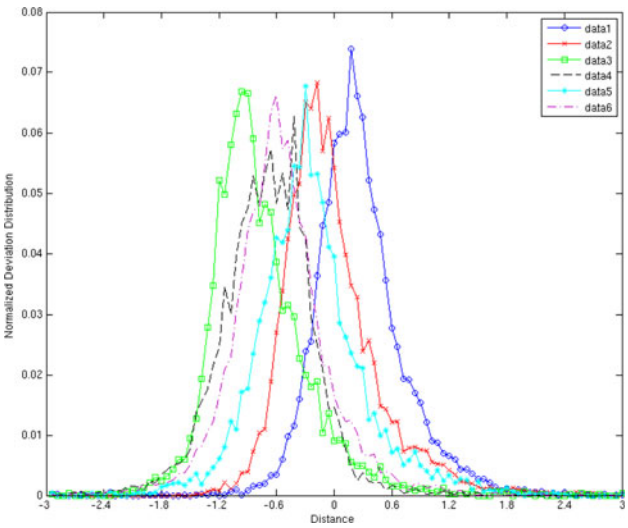

Fig. 2 Normalized deviation distribution of T1 and T2 jaws for Data#1 to Data#6

reproducibility of proposed methodologies has been shown by the similar results obtained from repeated experiments, and from different data sets.

References

[1] CA. Lascala, J. Panella, MM. Marques, *Analysis of the Accuracy of Linear Measurements Obtained by Cone Beam Computed Tomography,* Dentomaxillofacial Radiology, (2004) 33, 291-4

[2] P. Boulanger, C. Flores, JF. Ramirez, E. Mesa, JW. Branch, *Long Term Three Dimensional Tracking of Orthodontic Patients using Registered CBCT and Photogrammetry,* IEEE Eng Med Biol Soc, (2009) 2009, 3525-8

[3] M. Nielsen, C. Gramkow, S. Kreiborg, *Non-rigid Image Registration using Bone Growth Model*, Comp. Vision, VR and Robotics in Med and Comp-Assisted Surgery, (1997) 1205, 1-12

A Shape Model for Automated Recognition of Neutral Facial Expression in Surface Scans of Infants with Cleft Lip and Palate

T.A. Darvann[1], N.V. Hermann[2,1], P. Larsen[1], P. Lindholm[3], M. Andersen[3], H. Schatz[4], S. Kreiborg[1,4,5]

[1]3D Craniofacial Image Research Laboratory (School of Dentistry, University of Copenhagen; Centre of Head and Orthopaedics, Copenhagen University Hospital Rigshospitalet; and DTU Informatics, Technical University of Denmark), Copenhagen, Denmark

[2]School of Dentistry, University of Copenhagen, Pediatric Dentistry and Clinical Genetics, Copenhagen, Denmark

[3]Copenhagen University Hospital Rigshospitalet, Department of Plastic and Reconstructive Surgery, Copenhagen, Denmark

[4]School of Dentistry, University of Copenhagen, Cephalometric Laboratory, Copenhagen, Denmark

[5]Copenhagen University Hospital Rigshospitalet, Department of Clinical Genetics, Copenhagen, Denmark

Keywords Face recognition · Cleft lip and palate · 3D surface scanning · Facial expression · Shape modelling

Purpose

Quantification of facial shape in infants with cleft lip and palate (CLP) is of interest for surgical planning and evaluation in the individual as well as for population studies in craniofacial biology and clinical genetics. Non-contact surface scanners are becoming increasingly available and popular for recording of the infant face due to the ability of quickly and accurately obtaining 3-dimensional shape without deformation due to external forces. Deformations of the face due to changes in facial expression are, however, still present. The exited states of facial expression vary around a relaxed or *neutral* expression representing a zero-level of excitation where the muscles in the face are relaxed. The neutral facial expression may be adopted as a reference expression that, in adult subjects, is the most repeatable expression in the sense that it can be reproduced when the subject is instructed to do so. Furthermore, the neutral expression is a commonly used expression for measurement, both for the purposes of surgery planning/evaluation and in studies of CLP phenotypes. Infants are, however, non-compliant towards producing specific facial expressions. A measurement error occurs whenever the recording takes place during a facial expression other than the reference expression. Acquiring the perfect neutral expression in an infant may be challenging, and usually acquisition of a number of images is necessary.

Automation of the subsequent selection of the neutral expression recordings would make the process objective, and in the newly developed so-called dynamic, 60 frames/s, systems, an automated (on- or off-line) process would be a necessity for efficient selection.

The purpose of the present contribution is to present a simple statistical point distribution model that is capable of discerning between a neutral expression and other facial expressions.

Methods

Facial surfaces of seven infants (mean age 4.2 months; range 3.5 - 5.2 months) with untreated unilateral cleft lip with or without palate were obtained using a 3dMDface system (3dMD, Atlanta, GA, USA) (acquisition time 1.5ms) with the child sitting on a parent's lap. The operator (a radiographer experienced in facial photography of children) acquired scans (a total number between six and twelve) until five scans with a facial expression judged as neutral had been obtained. Written consent was given and Helsinki Declaration applies to the study.

Before analysis, surfaces of infant faces with a right-sided cleft were mirrored. Thirty-one 3D landmarks (Fig. 1) were manually placed in the nose and mouth region of all 35 surfaces. A point-distribution model (PDM) based on principal components analysis (PCA) of the landmarks was constructed after the following observations had been made: (1) Among the five scans of each individual, many scans could be visually judged to be non-neutral; (2) Visually recognizing the most neutral face in each individual was relatively easy; (3) A neutral face tended to have a characteristic amount of height of the mouth region (not wide open or forced closed); (4) A neutral face tended to have a characteristic amount of width of the mouth region (no pout or smile/cry). Frontal views of all scans were scored by four observers (all familiar with cleft faces) on six-point scales in terms of height and width of the mouth region (Fig. 1). Average scores from all four observers were calculated. In addition, the observers identified the scan(s) with neutral expression in each individual.

The x, y and z coordinate components of the landmarks were subjected to PCA, after Procrustes alignment had been carried out. Normally, the principal components (PCs) are determined in terms of the eigenvectors of a covariance matrix formed by deviations of each shape from the global mean shape. However, since it could be observed that the individuals in the sample spanned a wide range of cleft widths as well as vertical extensions of the cleft, it was realized that the proper deviations to be input to the covariance matrix would be the deviations relative to the mean shape of each respective individual and not a global mean shape.

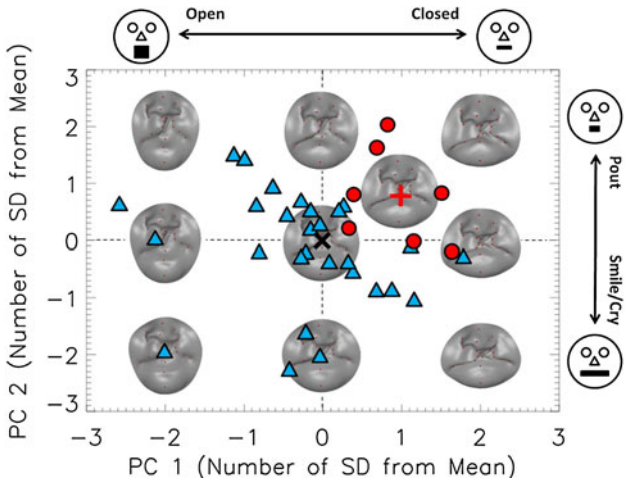

Fig. 1 Score plot for PCs 1 and 2. Triangle and circle symbols represent individual shapes. Circles represent scans with neutral facial expression. Synthetic surfaces of the mouth region are shown for the global mean shape (cross symbol) and for ±2SD from the mean along either PC. A synthetic surface capturing the shape of a neutral expression face is shown at the location of the plus symbol: the mean location of shapes with neutral facial expression. Landmarks are shown on each synthetic face scan. End-points of the visual scales used for scoring of the face scans are shown as smileys on the top and right side of the plot

Results

Synthetic face surfaces were created corresponding to the population mean shape, as well as for plus and minus 2 standard deviations (SD) from the mean, by forming linear combinations of the eigenvectors corresponding tp the first two PCs (Fig. 1). Correlation between PC 1 and visual scores of height of the mouth region was 0.67 (95% CI: [0.44, 0.82]). Correlation between PC 2 and visual scores of width of the mouth region was 0.60 (95% CI: [0.34, 0.77]). Surface scans that were identified by most observers as having the most neutral face in each of the seven individuals are plotted in Figure 1 as circles, demonstrating their confinement to a particular region of the score plot.

Conclusion

The score plot in Fig. 1 demonstrates that the constructed model provides a large degree of separation between faces with a neutral expression (circles) and faces with other expression types (triangles). This property of the model makes it suitable for automatic recognition of scans with a neutral facial expression. Although more sophisticated systems for facial expression recognition have been built, the simple statistical model presented here is to our knowledge the first to describe facial expression in CLP infants, as well as the first to address the particular task of recognizing neutral expression. The good separation capability of the model is due to the construction of a PCA covariance matrix using deviations relative to individual mean shapes instead of a global mean.

Computer assisted maxillary pre- and post-operative deformation analysis upon surgical distractive transversal expansion

C. Kober[1], S. Kannenberg[1], B. Frank[1], G. Al-Hakim[1], A. Parvin[1], C. Landes[2], R. Sader[2]
[1]HAW Hamburg, Faculty of Life Sciences, Hamburg, Germany
[2]University of Frankfurt, Frankfurt, Germany

Keywords Rapid maxillary expansion · Bone quality · Vestibular bone loss · New bone formation · 3D-reconstruction

Purpose

Severe maxillary compression with fontal dental crowding due to narrowness of the dentoalveolar base is associated with secondary tongue malpositioning, nasal breathing difficulty, speaking, and mastication problems. Transverse maxillary hypoplasia is most frequently seen in non-syndromal adolescents or adults but also in cleft lip palate and syndrome afflicted patients. Adult patients with progressed ossification of the median palatine suture suffering from unilateral or bilateral transverse hypoplasia can be treated effectively by means of surgically assisted rapid maxillary expansion (SARME). General indications for SARME are skeletal maturity regarding ossification of the palatal suture, marked transverse deficiency and dental crowding due to narrowed dentoalveolar base. To the authors' knowledge, there is no consensus in the literature regarding surgical technique, i.e. the amount and localization of osteotomies, the type of distractor, the existence, cause and amount of relapse, and whether overcorrection is necessary. By the surgical authors of this article, a new technique of tripartite osteotomy was developed as an alternative to median sagittal osteotomy.

Based on a clinical study, the outcome of several variants of SARME and distraction devices was analyzed by means of highly differentiated 3D-reconstruction and visualization with regard to displacement of skeletal tissue, new bone formation in the operation gap, and vestibular bone quality pre- and post-op. A detailed and systematic processing chain for pre- and post-operative evaluation of cranio-maxillofacial surgical treatment is presented. Though the applied techniques were partially explicitly developed for this purpose, the range of possible applications is much wider.

Methods

Patients: In the clinical study, 29 patients (18 male, 11 female) were included with mean age of 29 years from 16 years up to 44 years. There was one female cleft lip and palate patient and one male patient with congenital cleft lip and palate malformation. All patients were subjected to SARME with Le Fort I Osteotomy. In detail, the following operative approaches were applied

- Central or nearly central palatal sagittal osteotomy
- Two paramedian sagittal osteotomies between the later incisors and canines of the frontal maxillary bone and of the palate
- Tooth or bone anchored distraction devices
- Pterygoid osteotomy performed or omitted

Radiology: Pre- and post-operative high-resolution CT-data (SOMATOM Sensation 16 and Volume Zoom, Siemens Medical Solutions, axial image matrix 512 x 512 pixels, slice distance 0.5 - 0.6 mm) were acquired directly before and 6 - 11 weeks after SARME. All scanning parameters were chosen with respect to comparable distribution of gray values.

Computer aided processing: Firstly, a rigid registration of pre-op to post-op CT-data was performed using an iterative optimization algorithm with Euclidean distance as similarity measure. Thereafter, maxilla and palate including the gap due to osteotomy were semi-automatically segmented and reconstructed in 3D. For visualization of new bone formation in the operation gap, the voxels of the maxilla including surgical gap were isolated from the post-operative CT-data and subjected to highly transparent direct volume rendering with a special two color transfer function (Fig. 1). Finally, the 3D-models were *fragmented to selected anatomical regions* as vestibular and palatal bone, region around the operation gap, and pterygoid wings. By direct volume rendering using a physical color scale, the pre- and post-operative distribution of the Hounsfield values was qualitatively evaluated. By a comparison of the pre- and post-operative histograms of selected regions, a quantitative evaluation could be performed (Fig. 2). For image processing, 3D-reconstruction, and visualization, the toolbox Amira, Visage Imaging GmbH, Berlin, Germany, was applied.

Results

Technically, all methods proved applicability. New bone formation within the operation gap could be clearly differentiated from preexistent bone (Fig. 1). Finally, for the evaluation of bone quality, especially of vestibular bone, visual inspection allowed for significant qualitative conclusions whereas the histogram curves showed the quantitative applicability of the approach (Fig. 2).

From the medical point, palatal widening was proved for all patients by clinical measurements as well as by superposition of 3D-models based on the CT-data. For 25 patients, the skeletal tissue showed symmetrical appearance after surgery. Four cases were found with remarkable asymmetry, two single split osteotomy and two double spit osteotomy (Fig. 1). As regards new bone formation *in the operation gap*, we observed non-uniform bone formation along the osteotomy lines, but approximately symmetric (Fig. 1). The more symmetrical the osteotomy was performed, the easier the bone formation could be judged as symmetrical.

Both, the qualitative and the quantitative evaluation showed a remarkable degradation of the local distribution of the Hounsfield values from the CT-data after surgery besides for two cases. Thereby, a loss of bone mineralization was indicated again linked to remarkable reduction of structural parameters as Young's Modulus. This effect was especially observed for vestibular bone (Fig. 2). For the frontal region, also a decrease of bone quality was observed, but not as serious. For the pterygoid wings, no significant pre- and post-operative changes were observed. Interestingly, the bony structure of the palate was also less affected.

Discussion and Conclusion

Generally, all described methods could be successfully applied and showed reasonable results suitable for medical interpretation. Nevertheless, the semi-automatic segmentation was very laborious as needed in high quality. Due to bone weakened by surgical trauma, automatic methods weren't applicable. Severe problems were caused by metal artifacts for segmentation and for the quantitative analysis.

As regards the highly asymmetric post-operative outcome observed for four cases, there is the suggestion that it was due to an asymmetric sleeping position. The patterns of the newly formed bone suggest some influence of the surgical device, namely tooth or bone anchored, the kind of osteotomy, as well as of the applied forces for the distraction. For a final conclusion, further investigation is needed.

The results indicate that, by the presented processing chain, refined three-dimensional insight to the surgical outcome of the

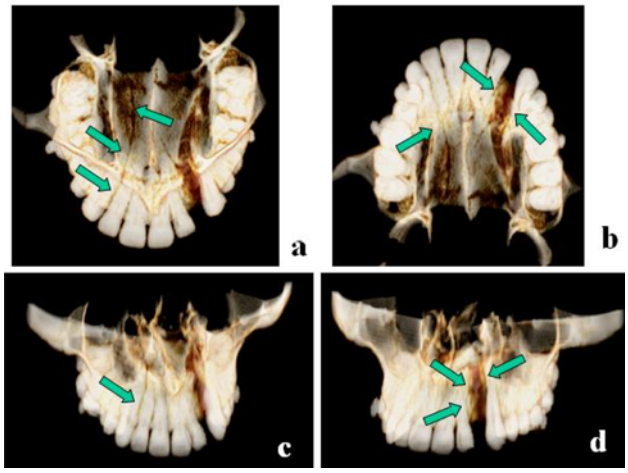

Fig. 1 Visualization of new bone formation of a highly asymmetric case, double split parasagittal osteotomy, view from **a** cranial, **b** palatinal, **c** frontal, **d** vestibular (male patient, 18 Y)

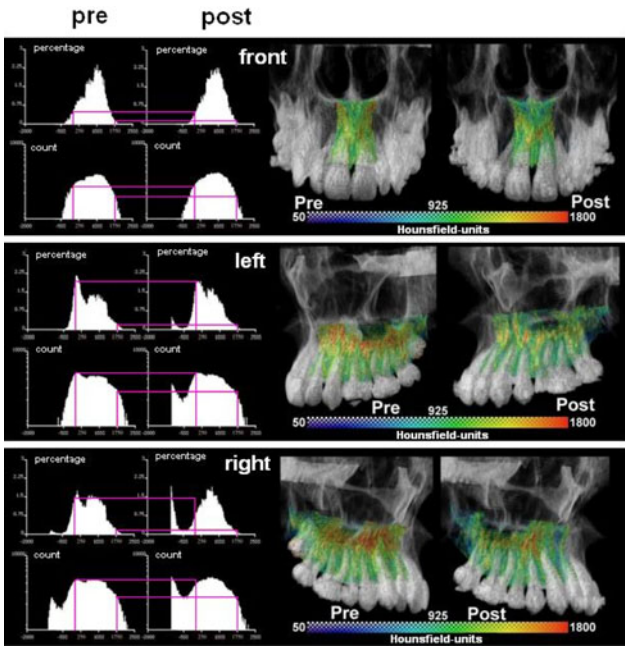

Fig. 2 Qualitative and quantitative comparison of the frontal section (top), the left vestibular section (middle), and the right vestibular section (bottom) of the maxilla

SARME can be gained concerning skeletal changes, progress of new bone formation, as well as vestibular bone loss being a common problem within this kind of treatment. Finally, as the overall processing chain proved applicability and significance it may be used for evaluation of further surgical approaches.

CBCT as a tool for Mandibular Third Molar evaluation on post-retention orthodontic patients

V Hernández-Soler
Valencia University, Spain

Keywords Mandibular third molars (M3) · Inferior alveolar nerve (IAN) · CT · CBCT and mandibular canal.

Purpose

To explore the visibility of CBCT imaging on the assessment of the impacted mandibular molars 20 consecutive retrospective orthodontic patients were evaluated. The results showed that CBCT cross-sectional images as well as reconstructed panoramic images gave a clear perception of the mandibular nerve. Anterior to M3 cross-sectional is the best view and posterior to M3, panoramic is the best view.

Until now panoramic radiograph has been used to assess third molar eruption[1]. Panoramic radiograph do not show the bucco-lingual position of the canal[2]. Given the difficulty of using panoramic films to identify the relationship between the canal and M3, it is not surprising that clinicians have sought out newer technologies as they become available. Although computed tomography (CT) has been available since the mid-1970s, it was not used routinely in dentistry[3456]. The advent of cone beam CT (CBCT) in the early 2000s reduced the cost and altered the cost-benefit analysis when comparing the radiation dose to the prospective information gained. Limited cone-beam CT has the advantages of high resolution and low dose and it is recognized as a useful tool because shows cortication of the mandibular canal. The purpose of this study is to explore the visibility of CBCT imaging on the assessment of the impacted mandibular M3 in retention orthodontic patients in which post-treatment panoramic x-rays suggest a risk for M3 impaction. Our specific aims were to evaluate the bucco-lingual relationship between mandibular M3 and the mandibular canal and to assess which view (panoramic, axial or cross-sectional) give better visibility for mandibular canal identification at different levels.

Material and Methods

20 consecutive retrospective patients (average age 21, 70% females) who had orthodontic treatment were evaluated. Subjects eligible for study enrollment were those who had possible risk of M3 impaction based on reviewing post-treatment panoramic radiographs. Limited CBCT, ICAT 8 cm, 30 seconds, 0.3 mm voxel size, 14 bits (Imaging Sciences International, Hartfield Pa) and software proprietary ICAT was used to assess M3-IAN relationship. Two observers evaluated the visibility and location of the mandibular canal in cross-sectional, panoramic and axial images at different levels (1 cm anterior to M3, at M3 and 1 cm posterior to M3). The physical relationship between the M3 and the IAN was classified into contact and separation and the distances between the mandibular M3 and IAN were measured twice by two observers.

Results

Inter and intra-observer is in good agreement (Kappa 0.76 for presence or absence and 0.9 for contact/separation).

The mandibular canal is viewed 100% on the anterior coronal views, commonly called anterior cross-sections. At M3 cross-sections is viewed 90% of the times and only 50% of the times on posterior cross-sectional. Posterior to M3, the canal is viewed on the panoramic view 90% of the times. On the panoramic at M3 and more anterior the canal is view 80% and 70% respectively. At all levels it was difficult to identify the canal by axial view (Table 1).

Only 2 subjects showed contact between the roots of the third molar and the mandibular canal by looking cross-sectional views. A close proximity of 1 mm (8, 40%), 1-2 mm (5, 25%) and 2-3 mm (2, 10%) was observed (Table 2).

The bucco-lingual position of the mandibular canal is not significant consistently located more to one side than the other in relation to M3 (Table 3)

Table 1 Canal identification

	Cross-sectional	Panoramic	Axial
ANTERIOR	20 (100%)	14 (70%)	2 (10%)
ATM3	18 (90%)	16 (80%)	0
POSTERIOR	10 (50%)	18 (90%)	1 (5%)

Table 2 Distance M3-Mandibular canal

	Contact	1 mm	1–2 mm	2–3 mm	>3 mm
Mandibular canal	2(10%)	8 (40%)	5 (25%)	2 (10%)	0

Table 3 Location IAN in relation to M3

Inferior		7 (35%)
Lingual		7 (35%)
Buccal		6 (30%)
Between the roots		0
Total		20
Inferior 7	Inferior–buccal	4
	Inferior–Lingual	3

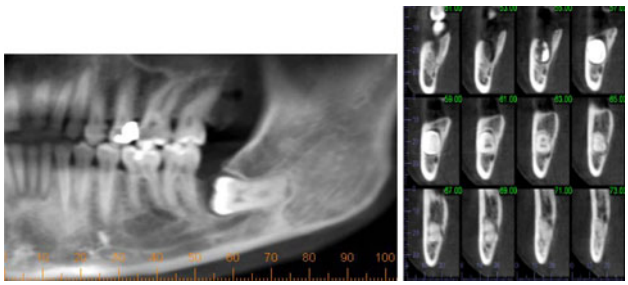

Discussion

An uncommon, but serious complication of mandibular third molars removal is injury to the IAN[7,8]. By using CBCT we can assess the anatomic relationship between proximity of the IAN canal and the M3 roots[10,11]. Second, we can ascertain the location of the IAN canal relative to the roots. Due to the close proximity of the mandibular canal and M3 and the lack of pattern for bucco-lingual position of both structures CBCT should be considered as a valid cost-benefit tool for planning before M3 removal. We find this information very useful for planning the operation and determining where it is safe to remove bone. The ability to trace the canal on the anterior cross-sectional view and on the panoramic view on the posterior ramous and to have it displayed on both, it is no trifling matter.

Conclusion

The results showed that CBCT cross-sectional images as well as reconstructed panoramic images gave a clear perception of the mandibular nerve. Anterior to M3 cross-sectional is the best view and

posterior to M3, panoramic is the best view. Cone beam technology improves the localization of IAN in relation to third molars and gives more information to the patient and to the surgeon for presurgical planning. Advanced 3D reconstruction to evaluate M3s provide information beyond that provided by panoramic images. This study confirmed the clinical usefulness of cone-beam CT for preoperative evaluation of impacted mandibular third molars.

References

[1] Blaeser BF, August MA, Donoff RB, et al. Panoramic radiographic risk factors for inferior alveolar nerve injury after third molar extraction. J Oral Maxillofac Surg. 2003;61:417

[2] Sick AL, Hammer WB, Shelton DW, et al. Complications following removal of impacted third molars. The role of the experience of the surgeon. J oral Maxillofac Surg. 1986;44:855.

[3] Maegawa H, Sano K, Kitagawa Y et al. Preopeartive assessment of the relationship between the mandibular third molar and mandibular canal by axial computed tomography with coronal and sagital reconstruction. Oral Surg Med Oral Pathol Oral Radiol Endod. 2003;96:639.

[4] Klinge B, Petersson A, Maly P. Location of the mandibular canal: Comparison of macroscopic findings, conventional radiography, and computed tomography. Int J Oral Maxillofac Implants. 1989; 4:327.

[5] Koong B, Pharoah MJ, Bulsara M. et al. Methods of determining the relationship of the mandibular canal and third molars: A survey of Australian oral and maxilofacial surgeons. Aust Dent J. 2006;51:64.

[6] Ohman A, Kivijarvi K, Blomback U, Flygare L. Pre-operative radiographic evaluation of lower third molars with computed tomography. Dentomaxillofacial Radiol 2006; 35:30.

[7] Miloro M, DaBell J. Radiographic proximity of the mandibular third molars to the inferior alveolar canal. Oral Surg Oral Med Oral Pathol Oral Radiol Endod 2005;100:545.

[8] Valmaseda-Castellon E, Berini-Aytes L, Gay-Escoda C. Inferior alveolar nerve damage after lower third molar surgical extraction: A prospective study of 1117 surgical extractions. Oral Surg Oral Med Oral Pathol Oral Radiol Endod. 2001;92:377.

[9] Miller CS, Nummikoski PV, Barnett DA et al. Cross-sectional tomography: A diagnostic technique for determining the buccolingual relationship of impacted mandibular third molars and the inferior alveolar neurovascular bundle. Oral Surg Oral Med Oral Pathol Oral Radiol Endod. 1990;70:791.

[10] Friedland B, Donoff B, Dodson TB. The use of 3-dimensional reconstruction to evaluate the anatomic relationship of the mandibular canal and impacted mandibular third molars. 2008;66:1678.

[11] Enciso R, Danforth RA, Alexandroni ES, Memon A and Mah J. Third molar evaluation with cone-beam computed tomography. Int J Comput Assit Radiol and Surgery. 2006; 1,2:113.